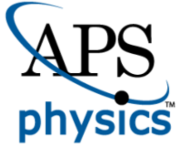

This is the accepted manuscript made available via CHORUS. The article has been published as:

Lack of quantum confinement in Ga_{2}O_{3} nanolayers

Hartwin Peelaers and Chris G. Van de Walle

Phys. Rev. B **96**, 081409 — Published 25 August 2017

DOI: 10.1103/PhysRevB.96.081409

Lack of quantum confinement in Ga_2O_3 nanolayers

Hartwin Peelaers[1,*] and Chris G. Van de Walle[1]

[1] *Materials Department, University of California, Santa Barbara, CA 93106-5050, USA*

Abstract

β-Ga_2O_3 is a wide-band-gap semiconductor with promising applications in transparent electronics and in power devices. β-Ga_2O_3 has monoclinic crystal symmetry and does not display a layered structured characteristic of 2D materials in the bulk; nevertheless, monolayer-thin Ga_2O_3 layers can be created. We used first-principles techniques to investigate the structural and electronic properties of these nanolayers. Surprisingly, freestanding films do not exhibit any signs of quantum confinement and exhibit the same electronic structure as bulk material. A detailed examination reveals that this can be attributed to the presence of states that are strongly confined near the surface. When the Ga_2O_3 layers are embedded in a wider band-gap material such as Al_2O_3, the expected effects of quantum confinement can be observed. The effective mass of electrons in all the nanolayers is small, indicating promising device applications.

β-Ga_2O_3 is a highly promising transparent conducting oxide, with transparency well into the UV owing to its large band gap of 4.8 eV,[1,2] enabling applications such as solar-blind deep-UV photodetectors[3,4] and contacts for solar cells.[5,6] The wide band gap, coupled with a small electron effective mass,[7,8] also makes Ga_2O_3 a promising material for high-power devices where a high break-down voltage is essential. Prototypes of high-voltage metal-semiconductor field-effect transistors[9] and Schottky barrier diodes[10] have been demonstrated.

β-Ga_2O_3 has a monoclinic crystal structure,[11] depicted in Fig. 1(a). The material can be mechanically cleaved, creating (100) surfaces.[12] Surprisingly, given the absence of any van der Waals gaps in this structure, it is possible to exfoliate β-Ga_2O_3, forming extremely thin layers.[13] Recently, such thin layers were used to fabricate high-voltage field-effect transistors.[14]

The conventional unit cell of β-Ga_2O_3 (Fig. 1) contains two symmetrically inequivalent Ga positions, and three inequivalent O positions. Two different (100) surfaces can be created.

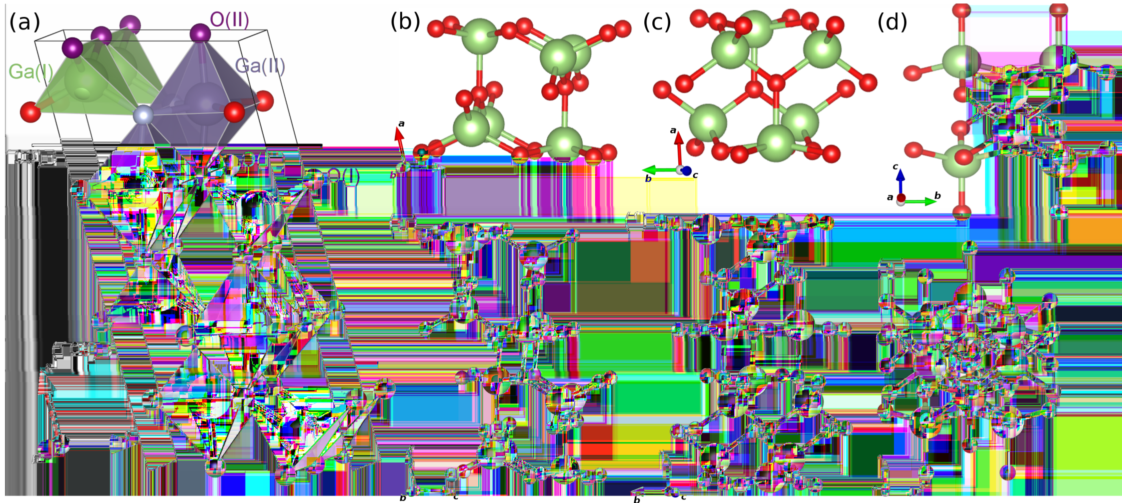

FIG. 1. (a) Crystal structure of β-Ga_2O_3 shown in the base-centered monoclinic 20-atom representation of the unit cell. The roman numeral labels refer to the three inequivalent O sites and the two inequivalent Ga sites. Ga(I) is tetrahedrally and Ga(II) is octahedrally coordinated. O(I) and O(II) are three-fold coordinated, while O(III) is four-fold coordinated. The (100)B surface planes are indicated by horizontal lines. (b)-(c) Two different side views and (d) a top view of a Ga_2O_3 nanolayer with thickness w=1. (e)-(f) Two different side views and (g) a top view of a Ga_2O_3 nanolayer with thickness w=2.

The most stable one is the (100)B surface,[15] which results from breaking two Ga(II)-O(III) bonds [bonds crossing the indicated (100)B line in Fig. 1]. The (100)A surface is located inbetween the indicated (100)B surfaces, and requires the breaking of 2 Ga(II)-O(II) bonds, which requires more energy compared to creating a (100)B surface.[15] The (100)B surface is indeed the one that is predominantly observed experimentally, e.g., in scanning tunneling microscopy (STM).[16]

Extremely thin Ga_2O_3 layers, with thicknesses on the order of monolayers, are expected to exhibit strong quantum-confinement effects—particularly since the electron effective mass is small. We use advanced first-principles techniques to investigate the atomic and electronic structure of freestanding nanolayers as a function of the layer thickness. Remarkably, the band structure of such layers is almost indistinguishable from the bulk. Based on a detailed examination of the electronic structure, we will be able to attribute the seeming lack of quantum confinement to the presence of electronic states associated with the surface. Unlike traditional surface states, which would tend to appear within the band gap and act as carrier traps, these Ga_2O_3 surface-related states behave essentially as highly conducting bulk states. We will compare and contrast the properties of freestanding layers with those of layers embedded within a wider-band-gap material such as Al_2O_3.

Our calculations are based on density functional theory using projector augmented wave potentials[17] as implemented in the Vienna *ab initio* simulation package (VASP).[18] The plane-wave basis set has an energy cutoff of 400 eV and a 1x8x4 **k**-point mesh is used. Traditional exchange-correlation functionals, such as the local density approximation or generalized gradient approximation, overly delocalize charge and lead to a large error in the band gaps; we therefore used a hybrid functional,[19,20] in particular the functional of Heyd, Scuseria, and Ernzerhof.[21,22] We used a mixing parameter of 35%, which we found to result in structural and electronic properties of bulk β-Ga_2O_3 that are very close to the experimental values.[7]

The smallest step size on the (100) surfaces was measured to be 5.3-6.2 Å by atomic force microscopy (AFM)[23,24] and 5.9 Å by STM,[16] which corresponds to half the conventional unit cell height, indicating that this is the smallest possible layer thickness of Ga_2O_3. Freestanding layers will have a thickness that is a multiple of this width; we call this multiple w. We will consider layers with thicknesses $w = 1$, $w = 2$, $w = 3$, $w = 4$, and $w = \infty$, the latter corresponding to bulk Ga_2O_3. Different views of the relaxed $w = 1$ and w=2 layers

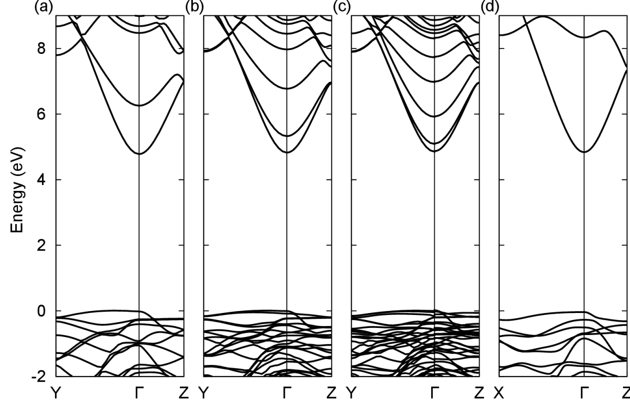

FIG. 2. Band structure of thin layers of Ga_2O_3 with thickness of (a) $w = 1$, (b) $w = 2$, and (c) $w = 3$. For comparison the band structure along the equivalent **k**-point path in bulk Ga_2O_3 ($w = \infty$) is shown in (d). The valence-band maximum is aligned to the vacuum level and set as the zero energy reference.

are shown in Fig. 1(b)-(g).

First we consider the $w = 1$ layer, which has a unit cell consisting of 4 Ga atoms and 6 O atoms. The surfaces contain Ga(II) (octahedral) and O(III) atoms. When the surface is relaxed, the Ga(II) atoms move inwards compared to the unrelaxed bulk positions, and the subsurface Ga (I) (tetrahedral) atoms move towards the surface. These relaxations are small (< 0.12 Å). This is similar to what was calculated for (100)B surfaces.[15] A similar relaxation occurs for the other layer thicknesses.

The Brillouin zone of the thin layers can be projected on a rectangle. We follow the convention of Ref. 15 and call Y and Z the high-symmetry points on the edge of the Brillouin zone in the [010] and [001] directions. The band structure for the w=1 layer along these two directions is shown in Fig. 2(a). The valence bands have a very small dispersion, similar to the bulk bands, since they are derived from O p orbitals. The conduction band is highly dispersive, with distinct s character, consisting of a mix of Ga and O s orbitals. The conduction-band minimum is located at the Γ point, while the valence-band maximum is located off Γ, making the thin layers indirect band-gap materials. However, the difference between the direct gap at Γ and the indirect gap is small (≤ 0.04 eV). This is very similar to bulk Ga_2O_3, where the band gap is also indirect, with a very small difference between the indirect and the direct gap.[7]

Fig. 2 shows that the band structures for layers with different thicknesses are all very

TABLE I. Band gaps (direct and indirect) and effective electron masses for Ga_2O_3 layers with different widths w. The indirect band gap occurs between the conduction-band minimum at Γ and a valence-band maximum on the Γ-Y line. For reference, the bulk values are also listed ($w = \infty$).

Width	Direct gap	Indirect gap	Mass Γ-Z	Mass Γ-Y
(w)	(eV)	(eV)	(m_e)	(m_e)
1	4.80	4.77	0.31	0.29
2	4.83	4.82	0.30	0.28
3	4.86	4.85	0.30	0.28
4	4.87	4.85	0.29	0.28
∞	4.88	4.84	0.29	0.28

similar, and comparable to the bulk band structure [Fig. 2(d)]. The valence-band maxima of all band structures are aligned on an absolute energy scale. The magnitude of the band gaps and the calculated effective electron masses are listed in Table I. The effective masses are virtually unchanged from their bulk values, and show only a small anisotropy. Both the direct and the indirect band gaps change only slightly as a function of layer thickness, in fact decreasing (by less than 0.1 eV) when the layer thickness is decreased. This is in stark contrast to the increase in band gap that is expected due the quantum confinement, particularly given that the conduction-band has a small effective mass (quantum confinement effects in the valence band are expected to be small due to the small dispersion).

This puzzling behavior can be explained by examining the nature of the conduction-band states. In Fig. 3(a)-(b) we show the charge density at the Γ point corresponding to the lowest two conduction bands, for the case of the $w = 2$ layer. The charge density of both bands is very similar, and clearly localized near the surface. This density includes a Ga dangling-bond state on the octahedral Ga(II) atom [whose bond with an O(III) atom was cut], and a band-like feature near the Ga(I) subsurface atom. The Ga(I) atom remains tetrahedrally coordinated and hence exhibits no dangling-bond states. We note that similar band-like features occur in the bulk Ga_2O_3 conduction-band states. For the lowest two conduction-band states in the $w = 2$ nanolayer, the band-like feature only occurs for the Ga(I) atoms near the surface, and not for the Ga(I) atoms in the interior; in the bulk, all Ga(I) atoms exhibit this band. The two next higher conduction-band states at the Γ point

are shown in Fig. 3(c)-(d). The third conduction-band state is spread out over the entire layer, and the fourth is mainly localized in the interior of the layer. Very similar charge densities are observed for the lowest conduction bands in the other nanolayers.

To quantify this further, we calculated the orbital-projected wavefunctions for each k-point and energy. We then compare the total projection on surface-Ga (sum of all orbitals for the four Ga atoms at the surface) with the total projection on interior-Ga atoms (normalized per Ga atom). Results of this procedure are shown in Fig. 3(e) for w=2 and in Fig. 3(f) for w=3. The color indicates which Ga atoms contribute most to each band. This information is not really meaningful for the valence bands, since they consist mainly of O p states, but we focus on the conduction bands. The two lowest conduction bands are mainly related to the surface-Ga atoms, in agreement with the density surfaces plotted in Fig. 3(a)-(b). The next two conduction bands [corresponding to the isosurfaces in Fig. 3(c)-(d)] are mainly related to interior-Ga atoms.

The splitting of these bands at the zone center decreases when the thickness of the layers increases [Fig. 2(a)-(c)]. The trend in the splitting can be attributed to the interaction of the two surface-related states across the thickness of the nanolayers. In thin layers, the distance between the two surfaces is small, the interaction is strong, and the splitting is large. When the thickness w is increased, the interaction between the surfaces is decreased and the splitting decreases.

The observed lack of quantum confinement in the nanolayers is, ultimately, the result of two counteracting physical effects. We have demonstrated that the lowest two conduction bands are very similar in nature; Fig. 2(a)-(c) show that the *average* of these states actually shifts upward as a function of decreasing thickness w, as we would expect from quantum confinement. The *splitting* of the states, due to the interaction across the thickness of the nanolayer, happens to decrease the energy of the lowest state by an amount that leaves the energy of the lowest conduction band almost unchanged as a function of layer thickness. This explains the seeming lack of quantum confinement for the lowest conduction band. The higher conduction bands *do* exhibit the effects of quantum confinement: they shift higher in energy with decreasing layer width, and there is no compensating pair-wise interaction between states.

Further light on the intriguing behavior of freestanding layers is shed by a comparison with the case of embedded layers. We examine thin layers of Ga_2O_3 surrounded by barrier layers

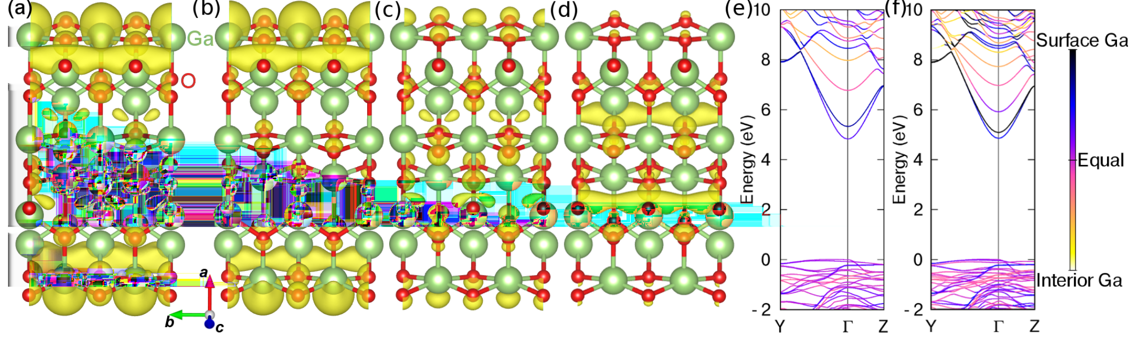

FIG. 3. Charge-density isosurfaces (corresponding to 10% of the maximum) for the $w = 2$ Ga_2O_3 layer calculated for (a) the lowest, (b) the second lowest, (c) the third lowest, and (d) the fourth lowest conduction band at the Γ point. For clarity, the cell is repeated twice in the b direction. (e)-(f) Projection of states in the band structure on surface-Ga atoms versus interior-Ga atoms. As indicated by the color scale, dark colors indicate predominantly surface-Ga character, light color interior-Ga character.

consisting of Al_2O_3. Al_2O_3 usually occurs in the corundum crystal structure,[25] but for the purposes of the present study we will consider heterostructures between Ga_2O_3 and Al_2O_3 with both materials in the monoclinic phase. We will study heterostructures consisting of a $w = 1$ layer of Ga_2O_3 and a $w = 3$ layer of Al_2O_3, and a $w = 2$ layer of Ga_2O_3 and a $w = 2$ layer of Al_2O_3. We assume that the in-plane lattice parameters (b and c) are constrained to those of Ga_2O_3. Full relaxation is allowed in the a direction. The calculated band structures for both cases are shown in Fig. 4(a)-(b).

The lowest conduction band is a Ga2O3 band, with Al character occurring only for higher energies, as confirmed by projected density-of-states calculations (not shown), consistent with the band alignment between Ga_2O_3[26] and Al_2O_3.[27] The valence-band maximum now occurs at the Z point, with density mostly residing on O atoms in the Al_2O_3 layer, while the valence band at Γ is spread out over O p states in both Ga_2O_3 and Al_2O_3 layer; this is consistent with the small magnitude of the valence-band offset.

The band gap is increased compared to a freestanding layer: for the heterostructure constrained to the Ga_2O_3 in-plane lattice parameters, the indirect (Z-Γ) gap increases to 5.35 eV and the direct (Γ-Γ) gap to 5.59 eV. The curvature of the conduction band is also modified, as the electron effective masses increase to 0.39 m_e along Γ-Z and 0.38 m_e along Γ-Y.

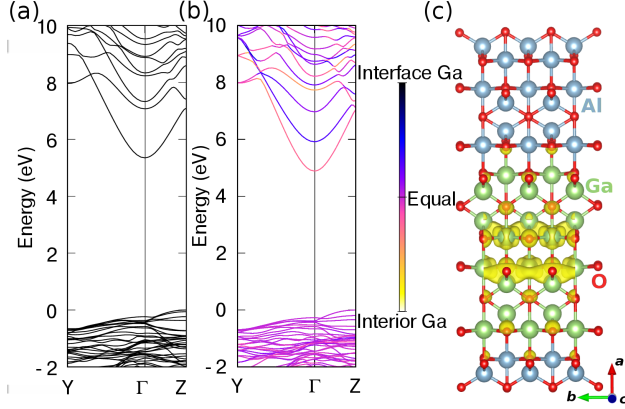

FIG. 4. (a) Band structure of a $w = 1$ Ga_2O_3 layer embedded in $w = 3$ layers of monoclinic Al_2O_3 with the in-plane lattice parameters constrained to Ga_2O_3. (b) Band structure of a $w = 2$ Ga_2O_3 layer embedded in $w = 2$ layers of monoclinic Al_2O_3 with the in-plane lattice parameters constrained to Ga_2O_3. The color scale indicates predominantly interface-Ga (corresponding to the four Ga atoms closest to the interface) character with dark colors, and interior-Ga character with light colors. (c) The isosurface corresponding to 10% of the maximum density of the lowest conduction band at Γ of the embedded layer with the lattice parameters constrained to Ga_2O_3 [corresponding to the band structure shown in (b)].

If the Ga_2O_3 is strained to the Al_2O_3 in-plane lattice parameters, the indirect band gap increases to 5.69 eV and the direct gap to 5.99 eV. This enhancement over the case of unstrained Ga_2O_3 occurs because the lattice parameters of Al_2O_3 are smaller than those of Ga_2O_3, and hence Ga_2O_3 undergoes a volume compression, which raises the conduction-band minimum. The electron effective masses increase to 0.43 m_e along Γ-Z and to 0.40 m_e along Γ-Y.

The difference between freestanding and embedded layers can be understood by inspection of the charge densities of the conduction-band states. Comparison of Fig. 3(a) with Fig. 4(c) shows that when the Ga_2O_3 layer is embedded, the Ga dangling bonds are removed. The band-like state above the tetrahedrally coordinated Ga atoms in the inner region is a bulk state, as discussed before. This is also evident from the atom-projected band structure [color scale in Fig. 4(b)], which shows that the lowest conduction band is mainly an interior-Ga state. Since the lowest conduction-band states in the embedded layers are states similar to bulk Ga_2O_3 states, these states are actually subject to quantum confinement, resulting in a

larger band gap for the $w = 1$ embedded layer [Fig. 4(a)] compared to the $w = 2$ embedded layer [Fig. 4(b)].

In conclusion, we used hybrid functional calculations to show that extremely thin freestanding Ga_2O_3 layers, with widths as small as 5.94 Å, do not exhibit any quantum confinement. We attribute this seeming lack of quantum confinement to the presence of conduction-band states associated with the surface layers. These states strongly interact, compensating for the quantum confinement. When the layers are embedded between Al_2O_3 barriers the band gap *does* show an increase due to quantum confinement. For freestanding layers, the band gap (∼4.8 eV) and electron effective masses (∼0.30 m_e) remain similar to the bulk values. In embedded layers the effective masses increase, along with the band gap, but they remain below 0.43 m_e. Such nanolayers, which can be created experimentally either by exfoliation or potentially by growth techniques such as molecular beam epitaxy, are therefore very promising for future devices.

ACKNOWLEDGEMENT

This work was supported by the Army Research Office (W911NF-13-1-0380) and by the MRSEC Program of the National Science Foundation (NSF) (DMR-1121053). Computing resources were provided by the Center for Scientific Computing at the CNSI and MRL: an NSF MRSEC (DMR-1121053) and NSF CNS-0960316, and by the Extreme Science and Engineering Discovery Environment (XSEDE), which is supported by NSF grant number ACI-1053575.

---

* peelaers@engineering.ucsb.edu

[1] H. H. Tippins, Phys. Rev. **140**, A316 (1965).

[2] T. Matsumoto, M. Aoki, A. Kinoshita, and T. Aono, Jpn. J. Appl. Phys. **13**, 1578 (1974).

[3] S. Nakagomi, T. Momo, S. Takahashi, and Y. Kokubun, Appl. Phys. Lett. **103**, 072105 (2013).

[4] T. Oshima, T. Okuno, N. Arai, N. Suzuki, S. Ohira, and S. Fujita, Appl. Phys. Express **1**, 011202 (2008).

[5] A. K. Chandiran, N. Tetreault, R. Humphry-Baker, F. Kessler, E. Baranoff, C. Yi, M. K. Nazeeruddin, and M. Grätzel, Nano Lett. **12**, 3941 (2012).

[6] T. Minami, Y. Nishi, and T. Miyata, Appl. Phys. Express **6**, 044101 (2013).

[7] H. Peelaers and C. G. Van de Walle, Phys. Status Solidi B **252**, 828 (2015).

[8] J. Furthmüller and F. Bechstedt, Phys. Rev. B **93**, 115204 (2016).

[9] M. Higashiwaki, K. Sasaki, A. Kuramata, T. Masui, and S. Yamakoshi, Appl. Phys. Lett. **100**, 013504 (2012).

[10] K. Sasaki, M. Higashiwaki, A. Kuramata, T. Masui, and S. Yamakoshi, IEEE Electron Device Lett. **34**, 493 (2013).

[11] R. Roy, V. G. Hill, and E. F. Osborn, J. Am. Chem. Soc. **74**, 719 (1952).

[12] M. Mohamed, C. Janowitz, I. Unger, R. Manzke, Z. Galazka, R. Uecker, R. Fornari, J. R. Weber, J. B. Varley, and C. G. Van de Walle, Appl. Phys. Lett. **97**, 211903 (2010).

[13] M. Albrecht, Private communication (2016).

[14] W. S. Hwang, A. Verma, H. Peelaers, V. Protasenko, S. Rouvimov, H. G. Xing, A. Seabaugh, W. Haensch, C. Van de Walle, Z. Galazka, M. Albrecht, R. Fornari, and D. Jena, Appl. Phys. Lett. **104**, 203111 (2014).

[15] V. M. Bermudez, Chem. Phys. **323**, 193 (2006).

[16] T. C. Lovejoy, E. N. Yitamben, N. Shamir, J. Morales, E. G. Víllora, K. Shimamura, S. Zheng, F. S. Ohuchi, and M. A. Olmstead, Appl. Phys. Lett. **94**, 81906 (2009).

[17] P. E. Blöchl, Phys. Rev. B **50**, 17953 (1994).

[18] G. Kresse and J. Furthmüller, Phys. Rev. B **54**, 11169 (1996).

[19] B. G. Janesko, T. M. Henderson, and G. E. Scuseria, Phys. Chem. Chem. Phys. **11**, 443 (2009).

[20] C. Freysoldt, B. Grabowski, T. Hickel, J. Neugebauer, G. Kresse, A. Janotti, and C. G. Van de Walle, Rev. Mod. Phys. **86**, 253 (2014).

[21] J. Heyd, G. E. Scuseria, and M. Ernzerhof, J. Chem. Phys. **118**, 8207 (2003).

[22] J. Heyd, G. E. Scuseria, and M. Ernzerhof, J. Chem. Phys. **124**, 219906 (2006).

[23] S. Ohira, N. Arai, T. Oshima, and S. Fujita, Appl. Surf. Sci. **254**, 7838 (2008).

[24] E. G. Víllora, K. Shimamura, K. Aoki, and N. Ichinose, J. Cryst. Growth **270**, 462 (2004).

[25] I. Levin and D. Brandon, J. Am. Ceram. Soc. **81**, 1995 (2005).

[26] H. Peelaers, D. Steiauf, J. B. Varley, A. Janotti, and C. G. Van de Walle, Phys. Rev. B **92**, 085206 (2015).

[27] M. Choi, A. Janotti, and C. G. Van de Walle, J. Appl. Phys. **113**, 044501 (2013).